Supporting materials

Table S1 Electronegativity, estimated band gap (E_g), conduction band edge (E_{CB}), and valence band edge (E_{VB}) for Bi_2WO_6 and CuS

Semiconductor	Electronegativity (eV)	E_{CB} (eV)	E_{VB} (eV)	E_g
Bi_2WO_6	6.36	0.41	2.48	2.89
CuS	5.25	–0.32	1.83	2.15

Table S2 The photocatalytic efficiency in single solution by various catalysts

Catalyst	Contaminant (concentration (mg/L))	Photocatalyst dosage (g/L)	Removal efficiency (%)	Time (min)	Reference
Bi_2WO_6/CuS-3	RhB(10)	1	99.9	105	This
	TCH(10)	1	74.7	105	This
	Cr(VI)(15)	1	75.7	105	This
Au/TiO_2/RGO	phenol(10)	0.2	> 90	240	(Lv et al., 2017)
SiO_2[MOYI]Cl–]Ag	AB92(20)	0.67	90	60	(Padervand et al., 2019)
Co_3O_4/Ag/Bi_2WO_6	Cr(VI)(40)	1	58	60	(Wan et al., 2019)
CNT-TiO_2	BPA(10)	0.5	100	30	(Hao et al., 2019)

Table S3 Comparison of the removal efficiency of RhB, TCH, and Cr(VI) mixture solution by various catalysts

Catalyst	Photocatalyst dosage(time)	Removal efficiency (concentration (mg/L))			Reference
		RhB	TCH	Cr(VI)	
Bi_2WO_6/CuS-3	1 g/L(105 min)	98.78%(10)	87.56%(10)	95.08%(15)	This study
RP-MoS_2/rGO	0.4 g/L(30 min)	99.3%(20)	/	98%(40)	(Bai et al., 2018)
$ZnFe_2O_4$/Na/bentonite	1 g/L(120 min)	94.2%(10)	/	88.6%(50)	(Guo et al., 2019)
BiOBr/Ti_3C_2	0.1 g/L(80 min)	97%(10)	/	96.2%(5)	(Huang et al., 2019)
Co_3O_4/Ag/Bi_2WO_6	1 g/L(120 min)	/	83%(10)	100%(40)	(Wan et al., 2019)

Table S4 The changes of pH before and after reaction in mixed system under the influence of initial pH

Initial pH	Final pH
2.19	1.78
3.94	5.24
5.59	6.71
8.10	7.59
10.18	8.03
12.30	12.05

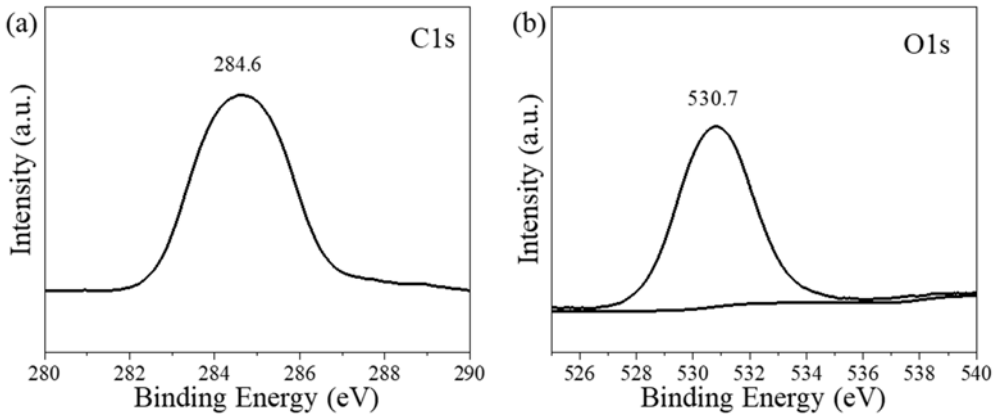

Fig. S1 XPS spectra of Bi_2WO_6/CuS-3: (a) C1s and (b) O1s

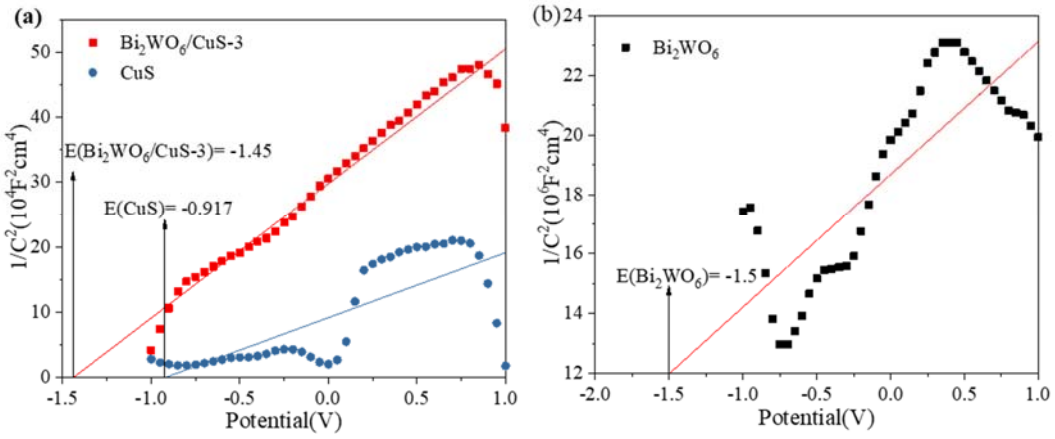

Fig. S2 Typical Mott-Schottky plots of Bi_2WO_6/CuS-3 (a) and Bi_2WO_6 (b)

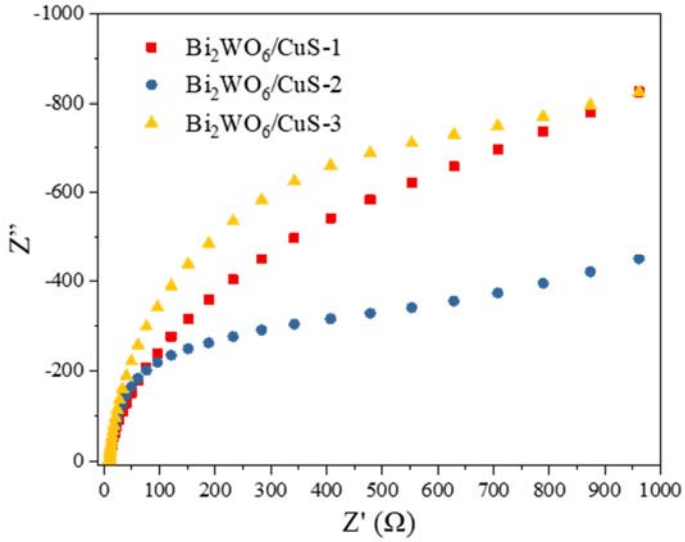

Fig. S3 EIS Nyquist of different photocatalysts

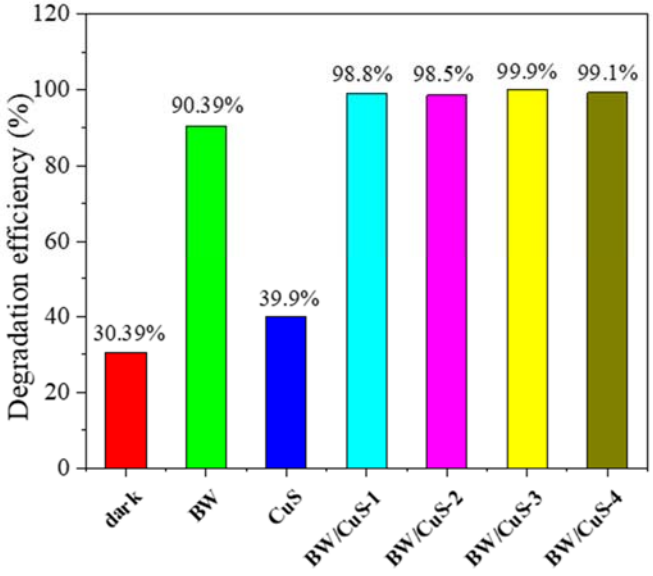

Fig. S4 The degradation efficiency of single RhB solution by different catalysts

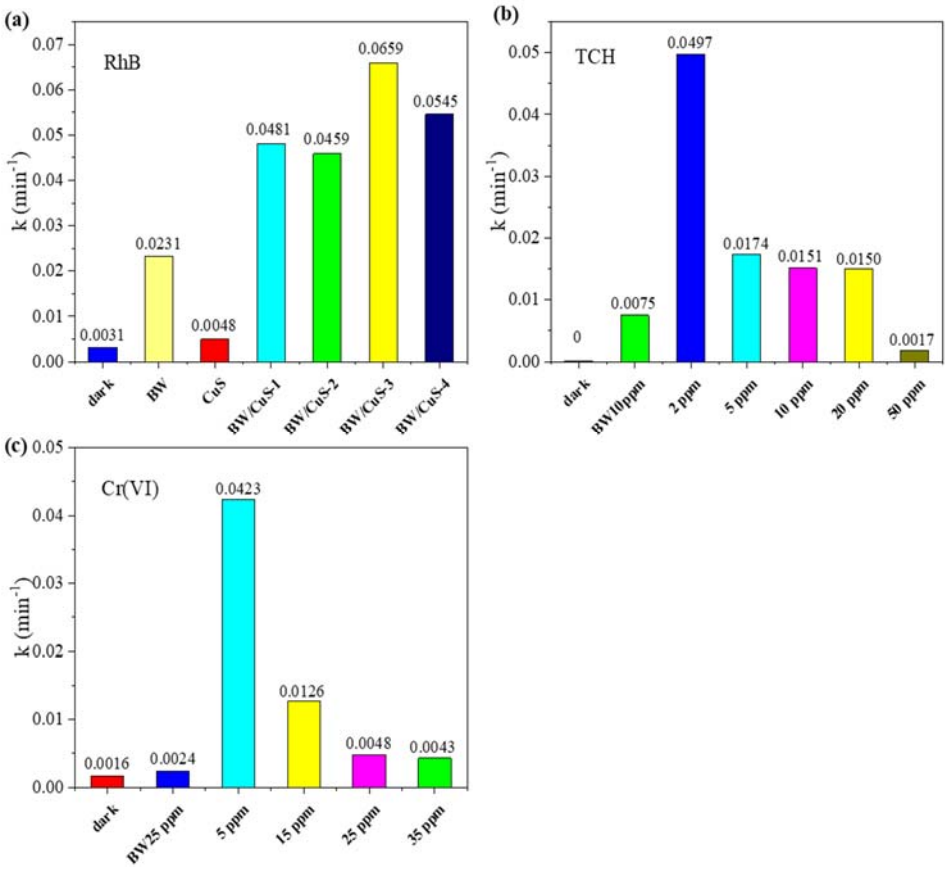

Fig. S5 The photocatalytic removal efficiency constants (K/min): (a) RhB, (b) TCH, and (c) Cr(VI)

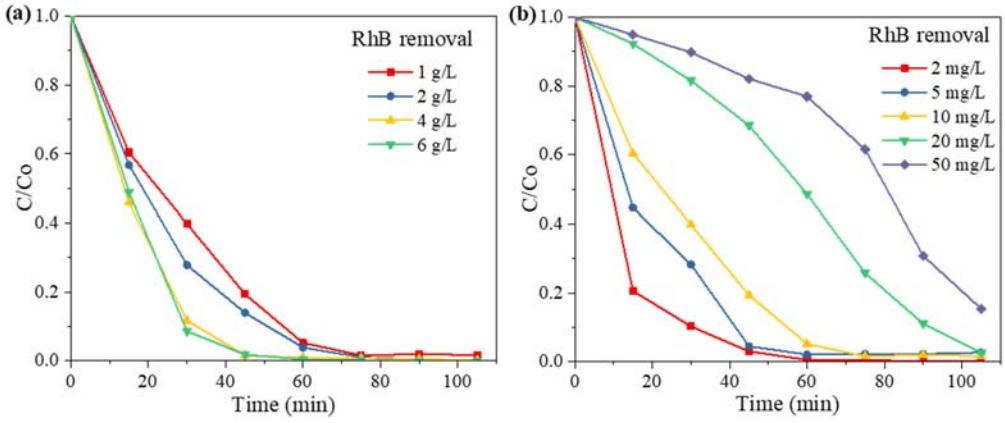

Fig. S6 Effect of (a) dosage of Bi_2WO_6/CuS-3 and (b) initial concentration of RhB

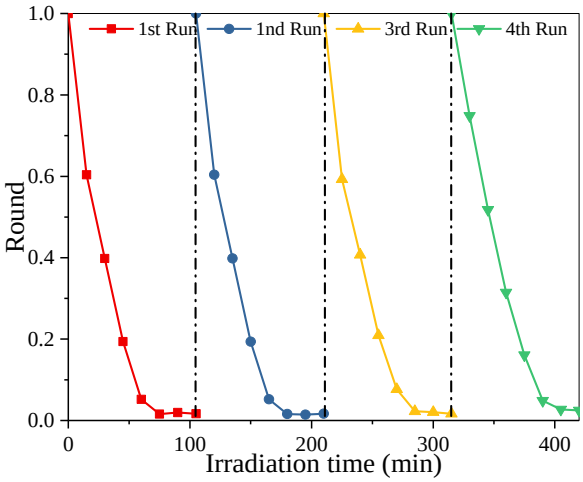

Fig. S7 Reusability of Bi_2WO_6/CuS-3 for photocatalytic degradation of RhB. (Experimental conditions: 0.1 g Bi_2WO_6/CuS-3, 100 mL 10 mg/L RhB solution)

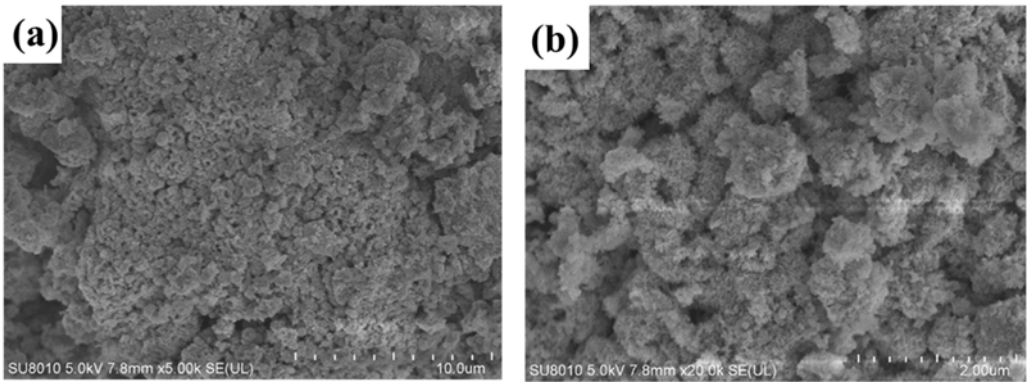

Fig. S8 SEM images of (a)–(b) of Bi_2WO_6/CuS-3 after photocatalytic degradation of RhB

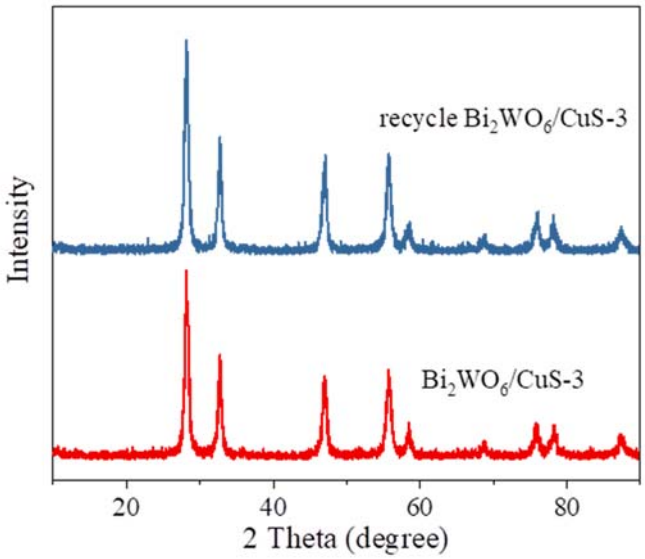

Fig. S9 XRD spectra of Bi_2WO_6/CuS-3 after photocatalytic degradation of RhB

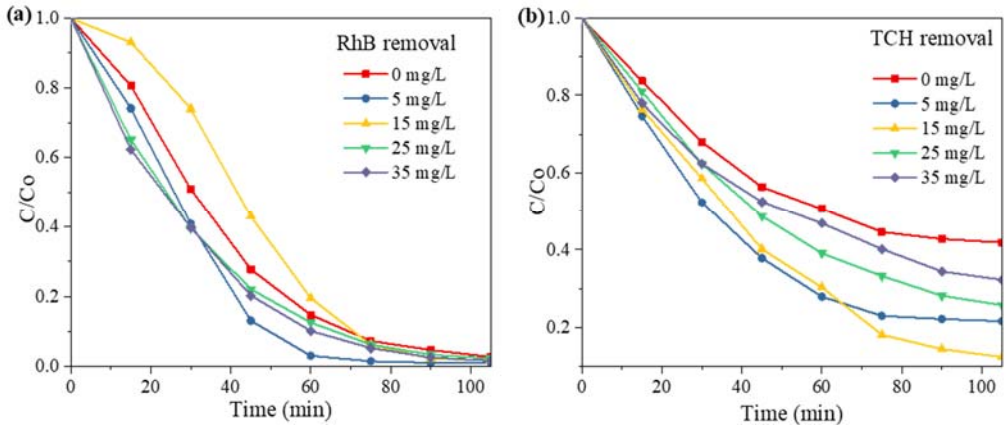

Fig. S10 Effect of Cr(VI) concentration for (a) RhB and (b) TCH. (Experimental conditions: 0.1 g Bi_2WO_6/CuS-3, 100 mL mixed solution, 10 mg/L RhB, 10 mg/L TCH, and 0–35 mg/L Cr(VI))

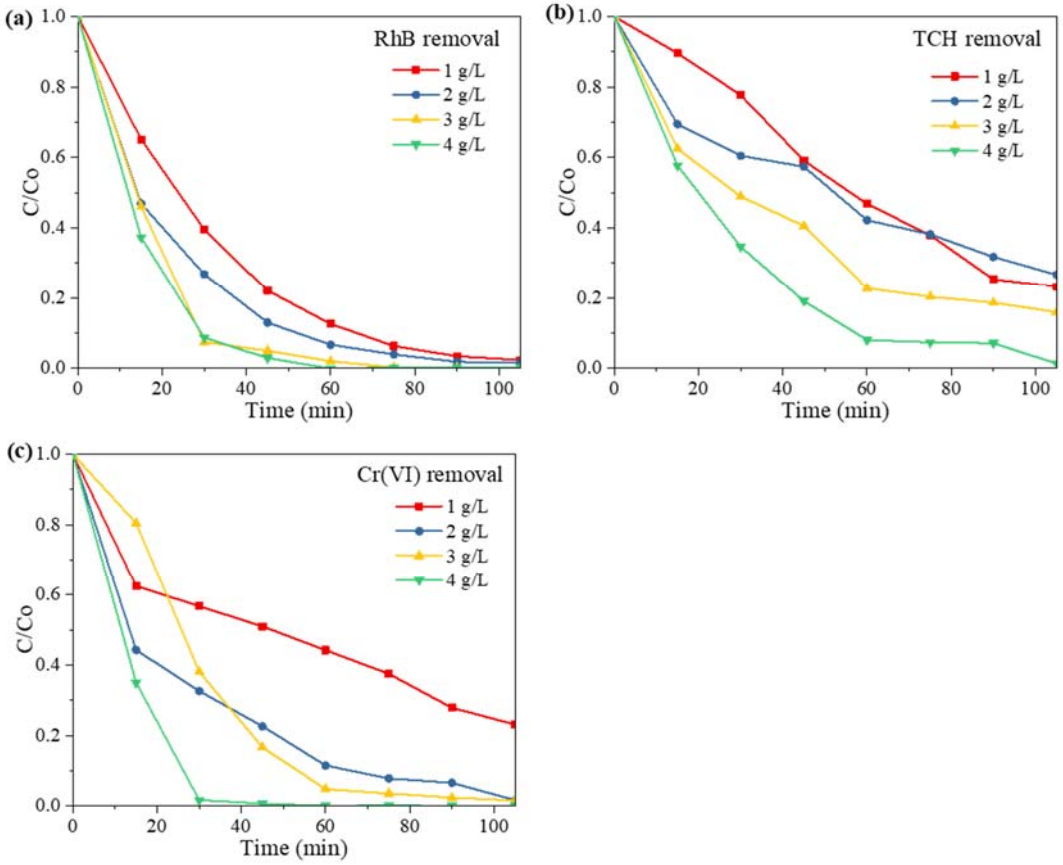

Fig. S11 Effect of catalyst concentration for (a) RhB, (b) TCH, and (c) Cr(VI). (Experimental conditions: 0.1–0.4 g Bi_2WO_6/CuS-3, 100 mL mixed solution, 10 mg/L RhB, 10 mg/L TCH, and 25 mg/L Cr(VI))

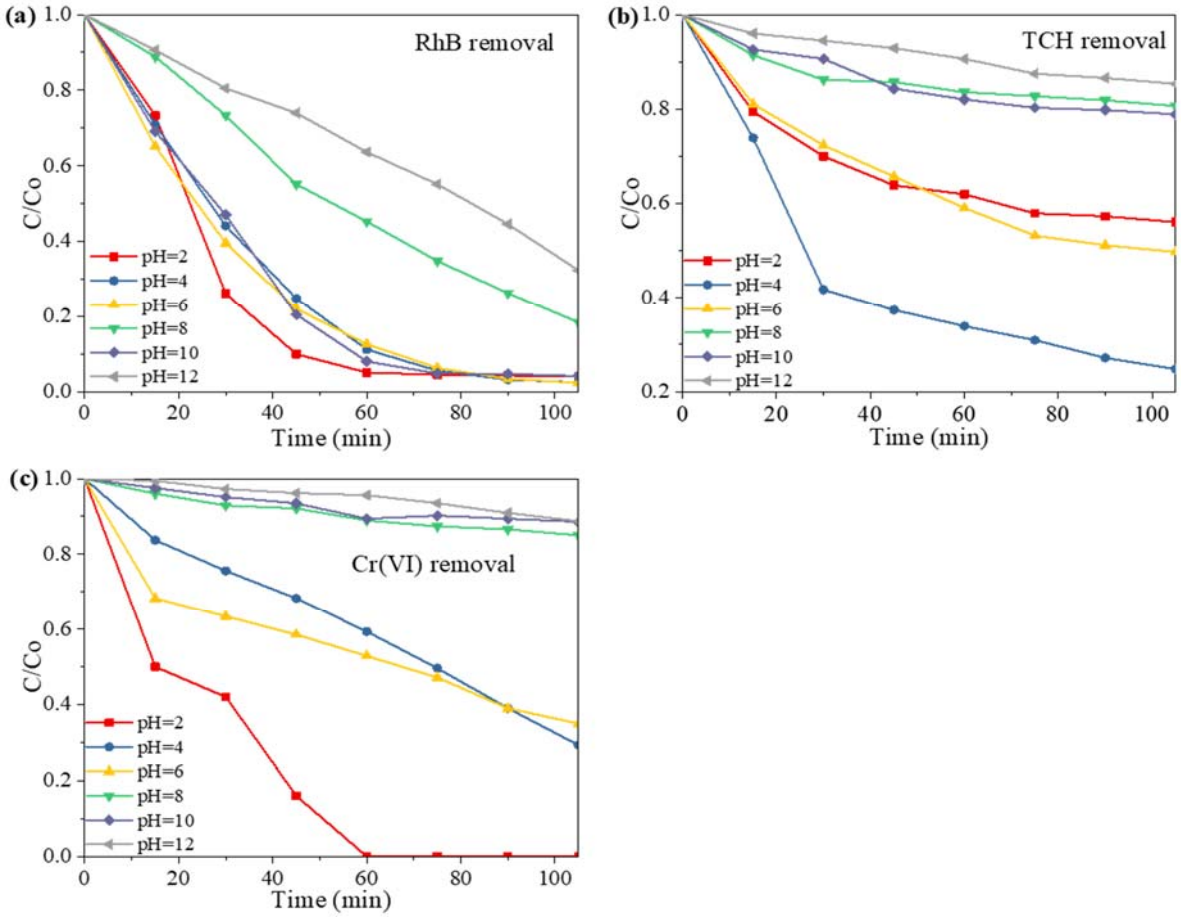

Fig. S12 Effect of initial pH for (a) RhB, (b) TCH, and (c) Cr(VI). (Experimental conditions: 0.1 g Bi_2WO_6/CuS-3, 100 mL mixed solution, 10 mg/L RhB, 10 mg/L TCH, and 25 mg/L Cr(VI))

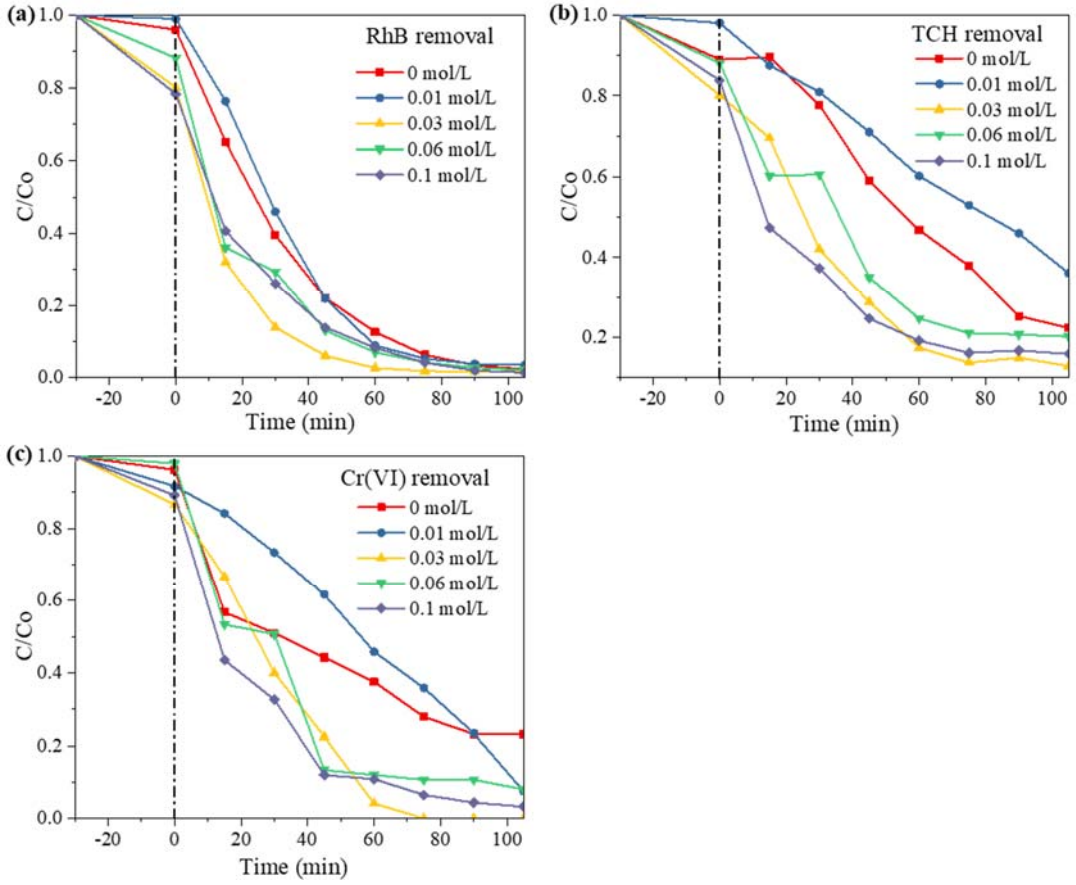

Fig. S13 Effect of glucose for (a) RhB, (b) TCH, and (c) Cr(VI). (Experimental conditions: 0.1 g Bi_2WO_6/CuS-3, 100 mL mixed solution, 0–0.1 mol/L glucose, 10 mg/L RhB, 10 mg/L TCH, and 25 mg/L Cr(VI))

References

Bai X, Du Y, Hu X, He Y, He C, Liu E, Fan J (2018). Synergy removal of Cr (VI) and organic pollutants over RP-MoS_2/rGO photocatalyst. Applied Catalysis B: Environmental, 239: 204–213

Guo Y, Guo Y, Tang D, Liu Y, Wang X, Li P, Wang G (2019). Sol-gel synthesis of new $ZnFe_2O_4$/Na-bentonite composites for simultaneous oxidation of RhB and reduction of Cr(VI) under visible light irradiation. Journal of Alloys and Compounds, 781: 1101–1109

Hao X, Wang G, Chen S, Yu H, Quan X (2019). Enhanced activation of peroxymonosulfate by CNT-TiO_2 under UV-light assistance for efficient degradation of organic pollutants. Frontiers of Environmental Science & Engineering, 13(5): 77

Huang Q, Liu Y, Cai T, Xia X (2019). Simultaneous removal of heavy metal ions and organic pollutant by BiOBr/Ti_3C_2 nanocomposite. Journal of Photochemistry and Photobiology A: Chemistry, 375: 201–208

Lv F, Wang H, Li Z, Zhang Q, Liu X, Su Y (2017). Fabrication and photocatalytic ability of an Au/TiO2/reduced graphene oxide nanocomposite. Frontiers of Environmental Science & Engineering, 12(1): 4

Padervand M, Asgarpour F, Akbari A, Eftekhari Sis B, Lammel G (2019). Hexagonal core–shell SiO_2[–MOYI]Cl–]Ag nanoframeworks for efficient photodegradation of the environmental pollutants and pathogenic bacteria. Journal of Inorganic and Organometallic Polymers and Materials, 29(4): 1314–1323

Wan J, Xue P, Wang R, Liu L, Liu E, Bai X, Fan J, Hu X (2019). Synergistic effects in simultaneous photocatalytic removal of Cr(VI) and tetracycline hydrochloride by Z-scheme Co_3O_4/Ag/Bi_2WO_6 heterojunction. Applied Surface Science, 483: 677–687